THE LEVEL STRUCTURE OF ^{163}Lu

THE LEVEL STRUCTURE OF ^{163}Lu

By

Nabil A.F. Lasheen

A Thesis

submitted to the School of Graduate Studies

in Partial Fulfilment of the Requirements

for the Degree

Master of Science.

McMaster University

January 1984

McMaster University

Hamilton, Ontario

Master of Science (1984)

(Physics)

Title: The Level Structure of ^{163}Lu.

Author: Nabil A.F. Lasheen, B.Sc. (Cairo)

Supervisor: Dr. J.C. Waddington.

Number of Pages: vii, 52

ABSTRACT.

The level structure of the Odd-A nucleus ^{163}Lu has been studied by the ^{148}Sm (^{19}F,4n) ^{163}Lu reaction through gamma-ray singles and gamma-gamma coincidence methods.

A number of rotational band structures have been observed up to a spin of 43/2. The backbending behaviour of the two signatures of the $h_{11/2}$ band, $\alpha = -1/2$ and $\alpha = 1/2$, has been observed. The critical frequencies for the backbends are $\omega_c = 0.264$ and 0.284 respectively.

Acknowledgement.

I would like to express my grateful appreciation to the following people:

Dr. J. C. Waddington, my supervisor, for his guidance in teaching me how to handle the problems I faced, and for his help during the writing of my thesis.

All the students in Dr. Waddington's group, for their help with my work.

All Tandem Accelerator Lab. (McMaster University) staff for their help, the preparing of targets, and the running of the FN accelerator and with the computer problems.

Miss Suzanna den Bleker, for her advice with the typing of this thesis.

The Physics Department, for their support.

TABLE OF CONTENTS

CHAPTER [1]

INTRODUCTION

A heavy ion reaction generally transfers a large amount of angular momentum, and hence populates high spin states in the residual nucleus.

Although many nuclei exhibit a simple rotational structure at low spins, many nuclei with large angular momentum show a deviation from this usual smooth trend. This so-called backbending behavior has been observed now in many nuclei at high spin.

Gamma ray spectra from high spin states are very complex with doublets and interference in gamma energies from different bands within the nucleus and from other residual nuclei. The present work describes the techniques used and the results obtained from a study of the high spin states of ^{163}Lu.

CHAPTER [2]

THEORTICAL DESCRIPTIONS

2.1 Introduction:

States with low angular momenta are often reasonably well known and understood in most nuclei. States with considerably higher angular momenta show a so-called "backbending" behavior which deviates from the usual rotation band rules. This adds a new dimension to nuclei at high spin which is now becoming better understood.

The following sections will describe the reasons suggested for backbending.

2.2 Nuclear Structure at large angular momentum:

The angular momentum has great influence on the nuclear structure in the yrast region. The yrast band is comprised of the states with lowest energy for a given angular momentum. In the yrast region the nucleus uses almost all its excitation energy to generate angular momentum.

A picture, Figure 2.1, presented by Bohr and Mottelson (1974), shows the relation between the nuclear phases as a function of the angular momentum, and the excitation energy. When moving along the yrast line, see Figure 2.1, several different nuclear domains can be

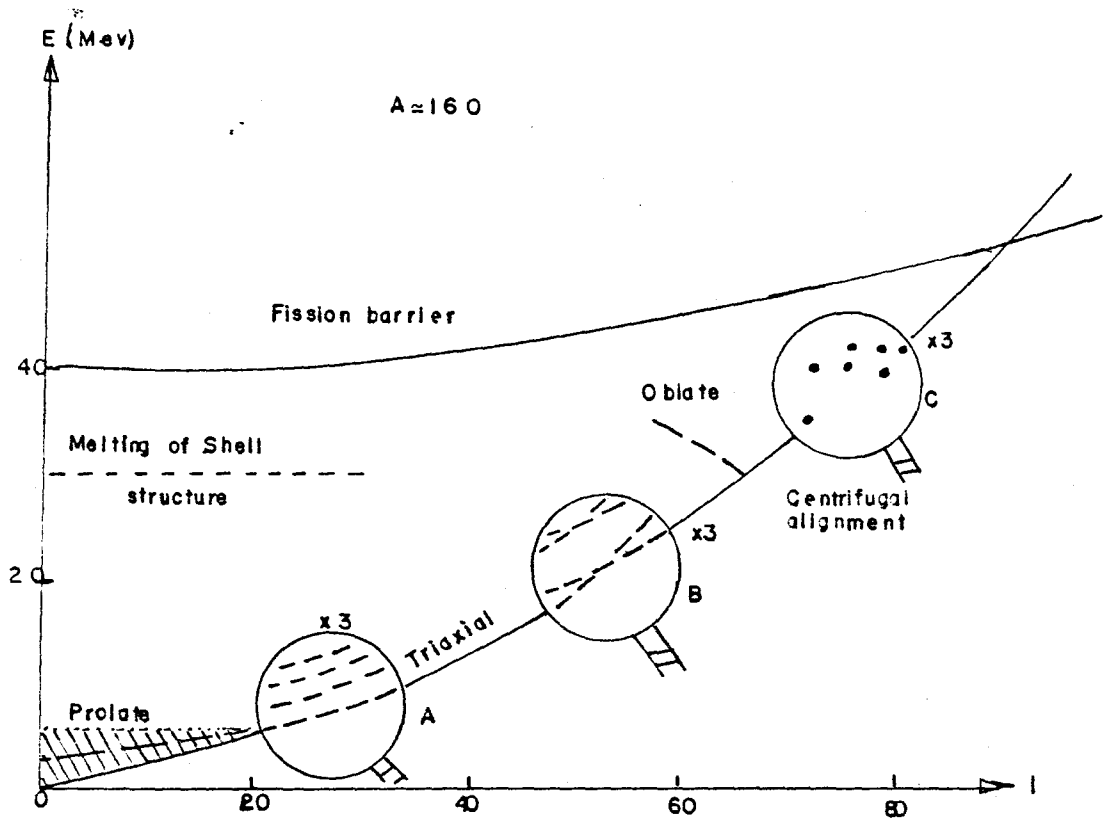

Figure 2.1 Schematic representation of the nuclear phases as a function of angular momentum and excitation energy.

recognized, which gradually merge into each other as the angular momentum increases. In the region of mass around 160, the nuclear ground states have a prolate symmetrical shape with deformation of $\beta \approx 0.3$ (see the hatched area in Figure 2.1). The spectrum for low angular momenta, consists of the rotational bands associated with collective rotation about an axis perpendicular to the symmetry axis.

When the nucleus rotates, the individual nucleons feel centrifugal and Coriolis forces. The Coriolis force tends to counteract the pairing force, so that the pairing correlations are reduced with increasing the rotational frequency. This effect has been called the Coriolis Antipairing effect [CAP]. The pairing correlations may break down completly at a certain critical angular momentum, when the Coriolis force becomes comparably strong to the pairing force.

Pairs of nucleons may be decoupled from the core by the Coriolis force and their angular momenta aligned along the axis of rotation.

Particles with large angular momenta feel the Coriolis force most strongly, and the breaking of one of those pairs seems to explain the experimentally observed increase of the moment of inertia with increasing rotational frequency. With increasing angular momentum, the nuclei enter the next region along the yrast line, for

regions A and B the centrifugal forces are driving the prolate nuclei into triaxial shapes. For larger angular momenta (region C) the nucleus acquires an oblate shape. Finally before the nucleus approaches fission at the upper end of the yrast line, it may pass through another phase of triaxial equilibrium shape.

2.3 Theory of rotational nuclei:

Some heavy nuclei have rotational levels. The energies for these levels approximately follow:

$$E_I=(\hbar^2/2\theta)\ I(I+1) \qquad 2.1$$

and their spacing is given by

$$\Delta E_{I,I-2}=(\hbar^2/\theta)(2I-1) \qquad 2.2$$

where I is the angular momentum and θ is the moment of inertia. At high spin, the rotational levels deviate from this behavior.

It was suggested that the nucleus undergoes a centrifugal stretching during rotation leading to a change of the nuclear moment of inertia, θ, but measurements of the change of the nuclear charge radius of the rotational states indicate that the change in the radius is smaller by one order of magnitude than necessary to predict the deviation of the rotational energies from the I(I+1) law. In a variable moment of inertia model, VMI, (Mariscotti, Scharff-Goldhaber and Buck (1969)) an improvement was obtained by expressing the energy by the two parameter formula

$$E_I(\theta)=(1/2)\ C(\theta-\theta_0)^2+(\hbar^2/2\theta)I(I+1) \qquad 2.3$$

where the first term is the potential energy, the parameters θ_0 and C are the ground-state moment of inertia and the restoring force constant. By applying the equilibrium equation

$$\partial E_I(\theta)/\partial\theta=0 \qquad 2.4$$

the moment of inertia θ for each state of spin I could be found. The angular frequency, ω, could be determined from the relation between the angular momentum and the moment of inertia as follows:

$$\hbar I=\theta\omega \qquad 2.5$$

and the angular frequency θ is related to the energy by

$$\partial E/\partial I=\theta \qquad 2.6$$

By expanding the rotational energy in powers of the angular frequency ω,

$$E_I=\alpha\omega^2+\beta\omega^4+\gamma\omega^6+\delta\omega^8+..... \qquad 2.7$$

A gradual increase of the moment of inertia with the angular frequency was obtained. The backbending effect might then be explained by crossing of two bands of different moments of inertia.

2.4 Strongly coupled bands in Odd-mass nuclei and their perturbation by the Coriolis effects:

Stephens and Simon (1972), presented a good comparison with a simple macroscopic system, to understand the Coriolis effects in rotating nuclei. A spinning wheel constrained to turn with a turntable, Figure

2.2a represents this situation. The Coriolis effects in the system manifest themselves as a force tending to align the axis of the wheel with that of the turntable, in such a way that the direction of rotation is the same in both. This arrangement is represented in Figure 2.2b.

The relevance of this system to the nuclear system is as follows. The spinning wheel represents a high spin particle in the nucleus, and the turntable represents the rotating deformed core. The symmetry (long) axis of a prolate core lies in the plane of the turntable. (This core rotates about an axis perpendicular to its symmetry axis.) The high spin particle is bound to the core in some way by the usual forces in the absence of rotation (Figure 2.2a).

As the nucleus rotates, the Coriolis force tries to decouple the particle from the core and align it as in Figure 2.2b. For strongly deformed odd-mass nuclei, the Coriolis coupling term can be considered as a perturbation of the hamiltonian equation, Stephens and Simon (1972)

$$H=H_{intr}+H_{rot}=H_{intr}+(\hbar^2R^2/2\theta) \qquad 2.8$$

where H_{intr} describes the coupling of the particle to the core. The total angular momentum,

$$\bar{I} = \bar{R} + \bar{J}$$

where $\bar{R}$ is the angular momentum of the rotation oriented

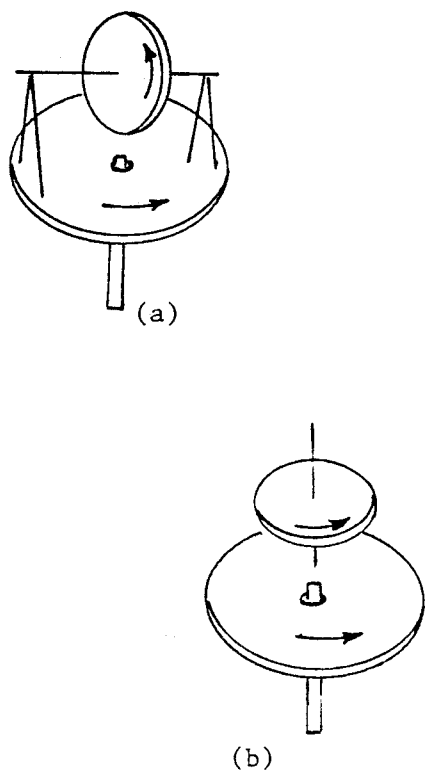

Figure 2.2 The Coriolis effects on spinning wheel constrained to turn with a turntable.

perpendicular to symmetry axis, and $\bar{J}$ is the particle angular momentum (see Figure 2.3).

$$H = H_{intr}+(h^2(\bar{I}-\bar{J})^2/2\theta)$$

$$= H_{intr}+(h^2/2\theta)[I^2-2\ \bar{I}.\bar{J}+\ J^2]$$

Using the fact that $I^2=I(I+1)$, $J=j$ and $I_z=J_z=K$

$$H = (\hbar^2/2\theta)[I(I+1)-K^2]+H_c+H_{intr}$$

$$+(\hbar^2/2\theta)[J^2-K^2] \qquad 2.9$$

where H_c is the Coriolis coupling, and K is the projection of the total angular momentum I on the symmetry axis. The Coriolis coupling term can be identified as follows

$$H_c = (-\hbar^2/\theta)\ \bar{I}.\bar{J} \qquad 2.10$$

Its matrix element is

$$\langle I,\Omega\pm1 \mid H_c \mid I,\Omega\rangle = (-\hbar^2/2\theta)\ [(I\mp K)(I\pm K+1)]^{1/2}$$

$$\langle\Omega\pm1 \mid j_\pm \mid \Omega\rangle \qquad 2.11$$

where

$$\langle\Omega\pm1 \mid j_\pm \mid \Omega\rangle = [j(j+1)-\Omega(\Omega\pm1)]^{1/2}$$

and Ω is the projection of the single-particle angular momentum j on the symmetry axis.

In strongly coupled bands, the single particle is strongly coupled to the deformation axis. The single particle precesses around the symmetry axis with a frequency much larger than the rotational frequency.

The single particle motion follows the rotational motion and the projection Ω of the single particle angular momentum on the symmetry axis is a constant of

motion [Figure 2.3a]. With decreasing deformation of the odd-mass nuclei and with increasing the spin, the Coriolis effects on the extra particle increase according to equation 2.11. The coupling of the extra particle to the deformation axis becomes progressively weaker. The rotational frequency increases with the angular momentum and the particle can not follow the core rotation any longer. For a sufficiently strong Coriolis interaction, the spin of the single particle will decouple from the deformation axis, align along the axis of rotation and precess around this axis independent of the core rotation [Figure 2.3b]. Since in this case the single particle angular momentum tends to align with the rotational angular momentum of the core, it is also known as rotational alignment.

An important feature is that the rotational aligned coupling scheme applies if the Coriolis matrix element H_c is larger than the splitting of the Nilsson states

$E_{\Omega\pm1} - E_{\Omega}$, that is

$$(\hbar^2/2\theta)[(I \mp K)(I\pm K+1)]^{1/2} \langle \Omega\pm1 | j_{\pm} | \Omega \rangle > E_{\Omega\pm1} - E_{\Omega} \qquad 2.12$$

in other words if:

i) the total angular momentum I is large.

ii) the deformation β is small.

iii) the matrix element $\langle \Omega\pm1 | j_{\pm} | \Omega \rangle$ is large.

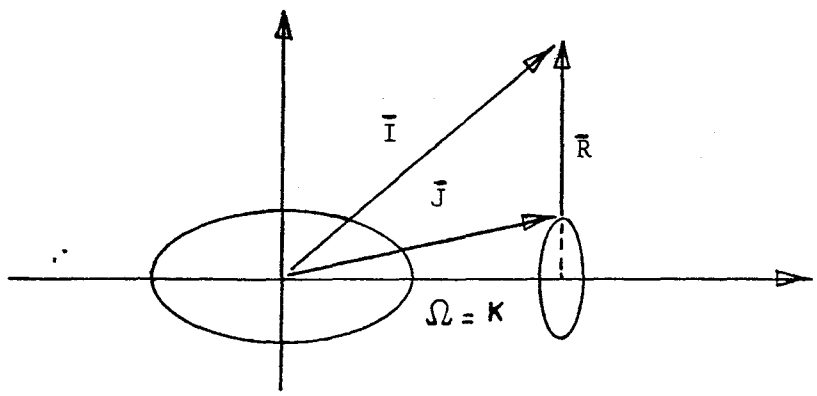

(a)

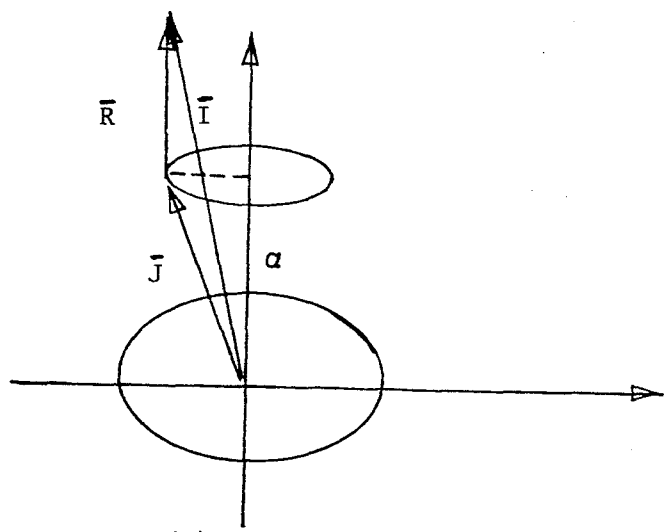

(b)

Figure 2.3 Schematic vector diagram of the strong-coupling scheme (a) and the rotation aligned coupling scheme (b).

2.5 The backbending effects in Odd-mass nuclei:

The backbending plot, (θvs.ω^2), shown in Figure 4.14, describes the behavior of the moment of inertia as a function of the rotational frequency for a rotational band.

An inspection of the backbending plot shows a slow and gradual increase of the moment of inertia at lower angular momenta, and a sudden change of the moment of inertia which gives this graph the name "backbending".

The moment of inertia and the rotational frequency are deduced from the energy spacing E_I-E_{I-2} of the transitions between rotational states of spin I and I-2 using the following equations:

$$2\theta/\hbar^2=[(E_I-E_{I-2})/4(I-j)-2]^{-1} \qquad 2.13$$

and

$$\hbar^2\omega^2 = [(I-j)^2-(I-j)+1][(E_I-E_{I-2})/2(I-j)-1]^2 \qquad 2.14$$

To improve the representation of the backbending curve for an odd nucleus the expectation value of the core angular momentum I-j is used. For a strongly coupled band, the expectation value of the angular momentum can be calculated as follows:

$$\langle I_x\rangle=[I(I+1)-K^2]^{1/2},\ I\neq K \qquad 2.15$$

where K is the projection of the angular momentum on the symmetry axis. The square of the rotational frequency for an even-even nucleus is given by

$$\hbar^2\omega^2=(I^2-I+1)[(E_I-E_{I-2})/(2I-1)]^2 \qquad 2.16$$

There is another way to represent the backbending curve, by plotting the expectation value of the angular momentum vs the angular frequency for each band.

From the rotation-alignment model, (Stephens, Diamond and Nilsson (1973) and Stephens (1975)), the energy is represented by

$$E_{rot-align}=(\hbar^2/2\theta)(I-\alpha)(I-\alpha+1) \qquad 2.17$$

where α = I mod 2.

CHAPTER [3]

EXPERIMENTAL TECHNIQUE

3.1 Introduction

This chapter will describe the apparatus and the techniques employed to obtain and analyse the data in this experiment to study ^{163}Lu with the ^{148}Sm [^{19}F,4n] ^{163}Lu reaction.

3.2 The Beam Transport System

A beam of fluorine-19 was produced as follows: fluorine ions from a duoplasmatron were made negative by passing them through a lithium adder gas, the ions were then extracted, focussed, and accelerated to the high voltage terminal [10.01 MV] of the Tandem accelerator at McMaster University.

At the terminal, the beam passes through a foil stripper, to become octa-positively charged [F^{+8}] and thereby subjected to a further acceleration.

On leaving the high energy end of the tank, the beam is focussed by a douplet of quadrupole lenses and defined by a set of object slits before entering the analyzing magnet, which transmits only particles of preselected rigidity.

The beam was then directed to the Lotus experimental area by the switching magnet, and a

number of quadrupole lenses and magnetic steerers which were strategically placed to guide the beam and focus it at the target position.

3.3 Target

The target for the experiment was a self supporting samarium foil isotopically enriched in ^{148}Sm. It was prepared by evaporating the metal from a mixture of samarium oxide and lanthanum filings onto a tantalum plate, where the lanthanum served as a reducing agent. The small globule of evaporated samarium was removed from the plate and cold rolled to the desired thickness, 2 mg per cm^2, and then covered on the back with ^{208}Pb to a thickness of 2 mg per cm^2, to stop recoil nuclei after the reaction.

3.4 Gamma-Events Analysis

This experiment was done with the standard techniques for multicoincidence experiments for high spin state reactions, which have been used in Tandem Accelerator lab.

Two types of detectors were used, five Ge[Li] detectors [Figure 3.1] and five NaI[Tl] detectors [Figure 3.2]. The Ge[Li] detectors were used to obtain high resolution spectra for the gamma transitions from the excited nuclei, ^{163}Lu and the NaI[Tl] detectors were used as the filtering system for the experiment.

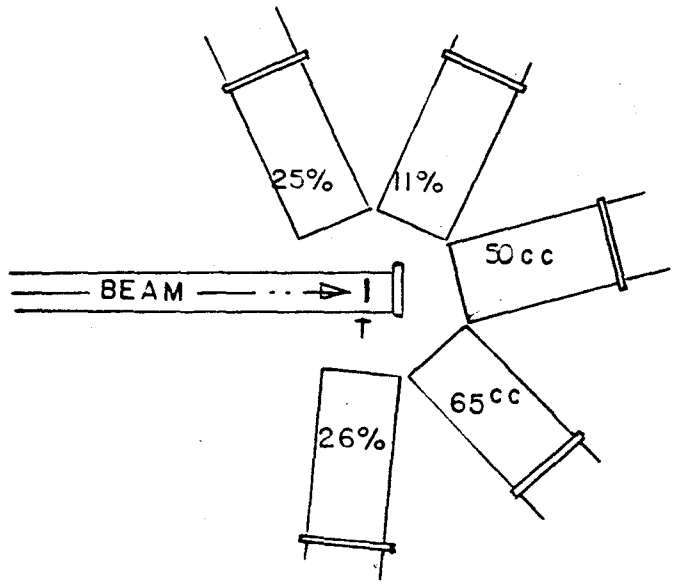

Figure 3.1 The Ge(1i) detectors arrangement, Horizontal plane.

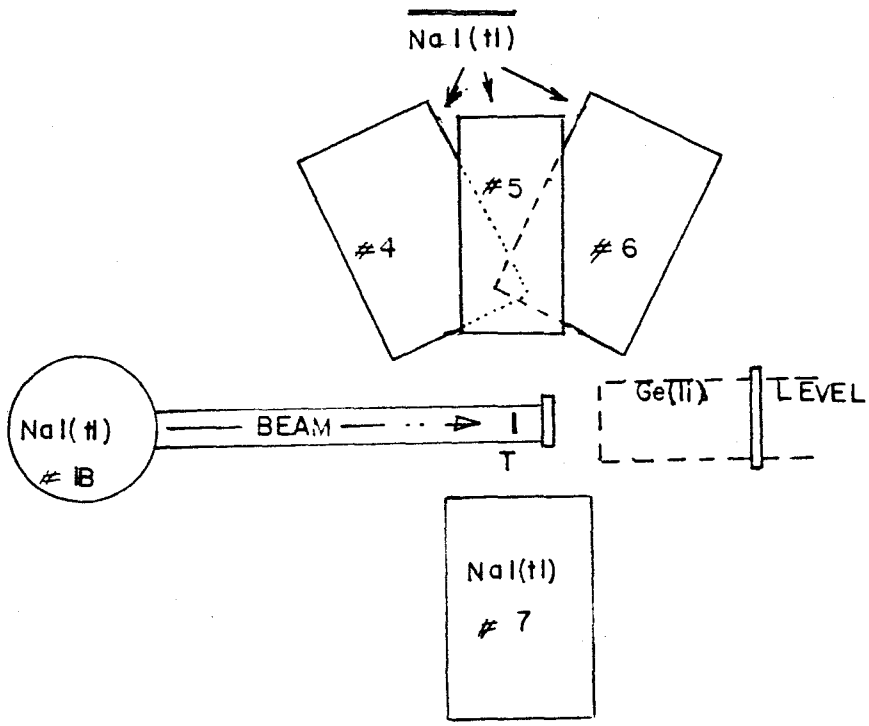

Figure 3.2 The NaI(tl) detectors arrangement.

i) Filtering System

The filtering system is a fast coincidence to select at least two events from two different NaI[Tl] detectors, out of five, to preferentially select long chains of gamma rays.

This system consisted of four NaI[Tl] crystals of size 5 inch diameter by 6 inch length, and one NaI[Tl] crystal of size 3 inch diameter by 3 inch length.

The detectors were arranged to cover a large solid angle around the target, as shown in Figure 3.2. The sides of the detectors were covered by three cylindrical layers of Cu, Cd and Pb respectively, from the surface of the detector, to minimize the detection of scattered gamma-rays, and also the faces of the detectors were covered with thin circular sheets of Cu, Cd and Pb, to absorb X-rays produced from the lead in the target.

When a gamma ray enters the detector and its energy is absorbed, the detector creates a [+ve] pulse corresponding to that energy. Then the pulse is analysed by a NaI[Tl] Fast Coincidence Unit, which has two outputs, the first which was used supplies a pulse if any coincidence is detected while the second supplies a pulse if any input is supplied.

The output of the Fast Coincidence Unit, (any coincidence), is connected to an input of an

Universal Coincidence, ORTEC 418A, as one of its inputs [Figure 3.3].

ii) Fast-Slow Coincidence System

This system was used to collect the coincidence gamma transitions. The system consisted of five Ge[Li] detectors arranged as in [Figure 3.1] and listed in Table 3.1. The sides and the faces of the detectors were covered with Cu, Cd and Pb respectively, as in the NaI[Tl] detectors and for the same reasons.

When an event enters the Ge[Li] detector, its energy may be absorbed and a pulse corresponding to that energy is created. The Ge[Li] output pulse is connected to a preamplifier, attached to the detector. The preamplifier output pulse is routed in two directions as follows [Figure 3.3]:

1. The preamplifier pulse serves as input for an amplifier, ORTEC 570, to give an amplified output pulse [+ve]. This amplifier output pulse is an input for a Linear Gate and Stretcher, ORTEC 442, which accepts a linear input pulse and generates an output pulse with amplitude equal to the input and shaped to a uniform rise time and width. The linear gate and stretcher output is connected as a direct input for an A.D.C.

2. The preamplifier output pulse is connected as an input for a Timing Filter Amplifier,

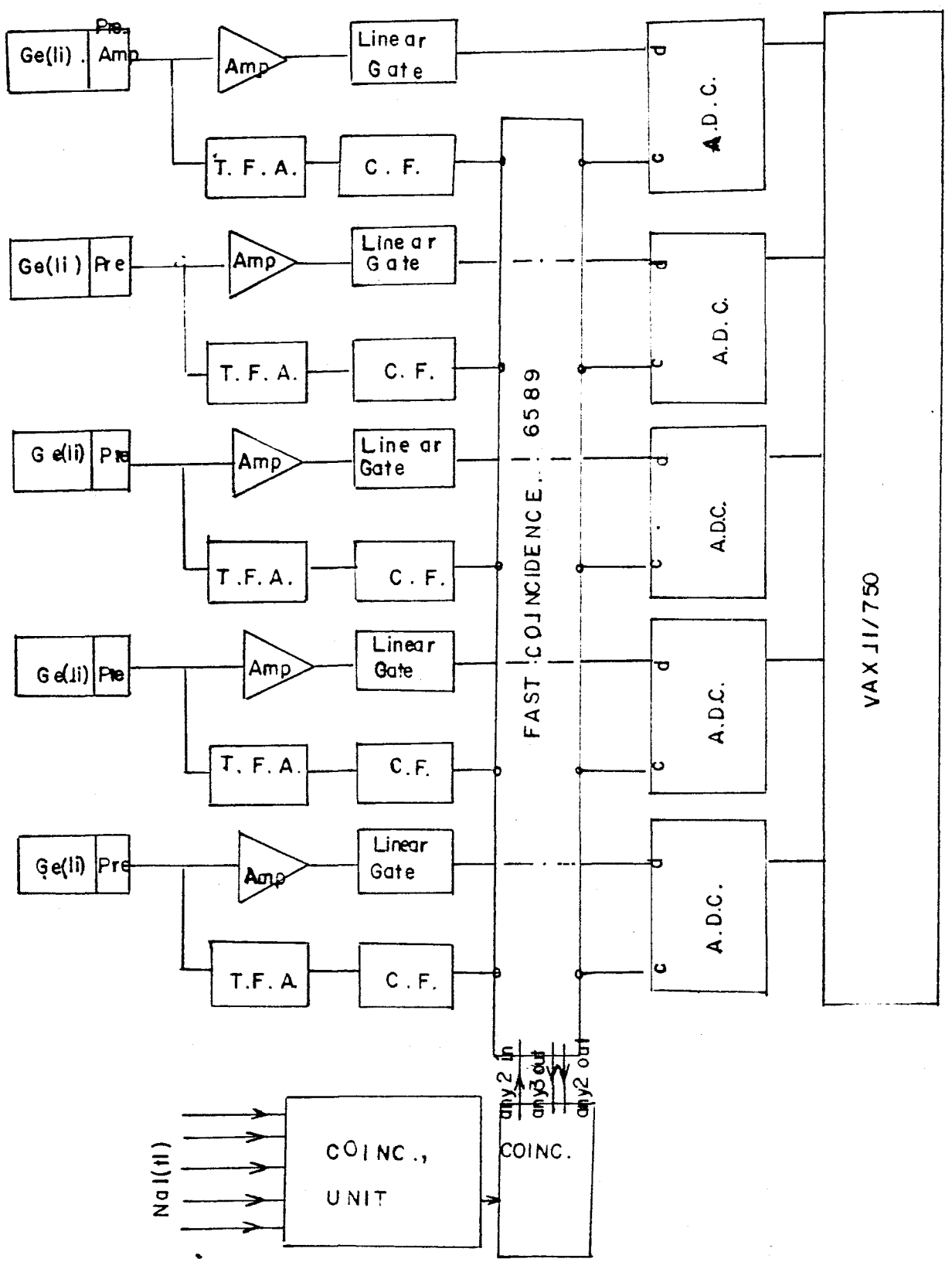
Ge(li)
Pre. Amp
Amp
Linear Gate
T. F. A.
C. F.
A.D.C.
Ge(li)
Pre
Amp
Linear Gate
T. F. A.
C. F.
A.D.C.
Ge(li)
Pre
Amp
Linear Gate
T. F. A.
C. F.
A.D.C.
Ge(li)
Pre
Amp
Linear Gate
T. F. A.
C. F.
A.D.C.
Ge(li)
Pre
Amp
Linear Gate
T. F. A.
C. F.
A.D.C.
FAST COINCIDENCE 6589
VAX 11/750
any2 in
any3 out
any2 out
COINC.
COINC., UNIT
NaI(Tl)

ORTEC 474, which shapes pulses and permits optimization of the signal to the noise ratio. Its output [+ve] shaped pulse is connected as input for a Constant Fraction Discriminator, ORTEC 473, which provides logic signals. The C.F.D. output shaped pulse is connected to one of the inputs of a Fast Pentad Coincidence, 6589 (manufactured at McMaster University).

The Fast Pentad Coincidence has two outputs, any two inputs in coincidence and any three inputs in coincidence. Those two outputs were connected as inputs for an Universal Coincidence, ORTEC 418A, which has now three inputs, two inputs from the Fast-Slow coincidence system, Fast Pentad Coincidence, and an input from the Filtering system, NaI[Tl] Fast Coincidence Unit.

The Universal Coincidence was switched for an output of any two inputs in coincidence, this output was fed back to Fast Pentad Coincidence, 6589, to produce gating pulses for the coincidence input to the ADCs.

The data collected from the A.D.C.s are transferred to a VAX11/750.

3.5 The Experiment:-

After a description of the technique and the electronic units used, a description of the experiment will be given.

This experiment was designed to study ^{163}Lu at high spin states. To get ^{163}Lu, the ^{148}Sm [^{19}F, 4n] ^{163}Lu reaction was used. ^{163}Lu is not the only heavy nucleus produced by the fluorine beam, so a good choice of the beam energy of ^{19}F is very important, to obtain the reaction needed with a high probability and reduce the probability for the other reactions.

To do that, a simple formula depending upon masses of the target and the projectile, the Q-value and the coulomb energy, can give some idea about the appropriate beam energy.

This formula is

$$E_x = E_b - E_{cm} + Q \qquad [i]$$

Where E_b is the beam energy

E_{cm} is the energy of the center of mass

Q is the Q-value of the reaction

and E_x is the excitation energy

$$E_{cm} = m_t E_b/[m_b + m_t] \qquad [ii]$$

$$E_c = Z_b Z_t/[r[A_b^{1/3} + A_t^{1/3}]] \qquad [iii]$$

where E_c is the coulomb energy and r =1.2 fm.

m_t, Z_t and A_t are the atomic mass, atomic charge and atomic number for the target.

m_b, Z_b and A_b are the atomic mass, atomic charge and atomic number for the projectile.

Working through those equations, the beam energy should be around 90 MeV for the reaction

$^{148}Sm[^{19}F,4n]^{163}Lu$. This leaves the residual nucleus with $\tilde{\sim}$ 16 MeV of excitation energy.

The experiment was run for a wide range of beam energies [85, 90, 95, and 100 MeV]. Singles spectra with the beam on and then off were made. These off-beam singles spectra gave the decay of the product nuclei of the reaction (Alkhazov et al (1979) and Berlovich et al (1980)).

A search was made for gamma transitions from the decay of ^{163}Lu, with a careful look at their intensities, to select the beam energy which produced the ^{163}Lu with highest probability. This was determined to be 90 MeV.

After determining the best beam energy, the apparatus was set-up as described previously for the coincidence experiment.

Using ^{57}Co (121.97 keV) and ^{137}Cs (661.595 keV), the amplifier gain was adjusted so that a conversion gain of 0.5 keV per channel was obtained.

An intensity calibration was made for each detector using a standard source with known relative intensities [^{152}Eu] at the same position as the target and with the same experimental arrangement. Then using those curves and the peak areas of ^{163}Lu lines, the relative intensities for the ^{163}Lu gamma-rays were found.

After testing everything, to verify that it was working fine, the experiment was run for a beam energy of 90 MeV and a beam intensity of 6 nA. The detector gains were checked every two and half hours, and gamma singles spectra were collected for each detector as well as gamma coincidences for selected gates. A record of the coincidence events was kept on tapes.

TABLE 3.1

DETECTOR	RESOLUTION
25% Coaxial	2.0 keV at 1332 keV
11% Coaxial	2.0 keV at 1332 keV
50cc Coaxial	2.5 keV at 1332 keV
65cc Coaxial	3.0 keV at 1332 keV
26% Coaxial	3.5 keV at 1332 keV

CHAPTER [4]

EXPERIMENTAL RESULTS FOR ^{163}Lu.

4.1 Introduction

Studies of the backbending behaviour of the rotational bands of high spin states have been made by many groups.

The nucleus ^{163}Lu has been studied by a group from Yale University, Rosenthal et al (1982), and their results are summarized in the level scheme shown in Figure 4.1, which gives an idea about the levels populated, gamma transition energies and their intensities. The present work describes a continuation of their work to higher spin.

A summary of the present work is shown in Figure 4.2, which is a level scheme for ^{163}Lu with more information than that of Figure 4.1.

4.2 Gamma ray singles Spectrum Measurements

The gamma ray singles spectrum is a record of all the events detected and is represented as the number of events vs gamma ray energy. Figure 4.3, is a gated singles spectrum (gated by the detection of a gamma ray in the NaI detectors), and it is a sum of the five Ge[Li] detector spectra. As explained previously, the detectors pulse height was adjusted

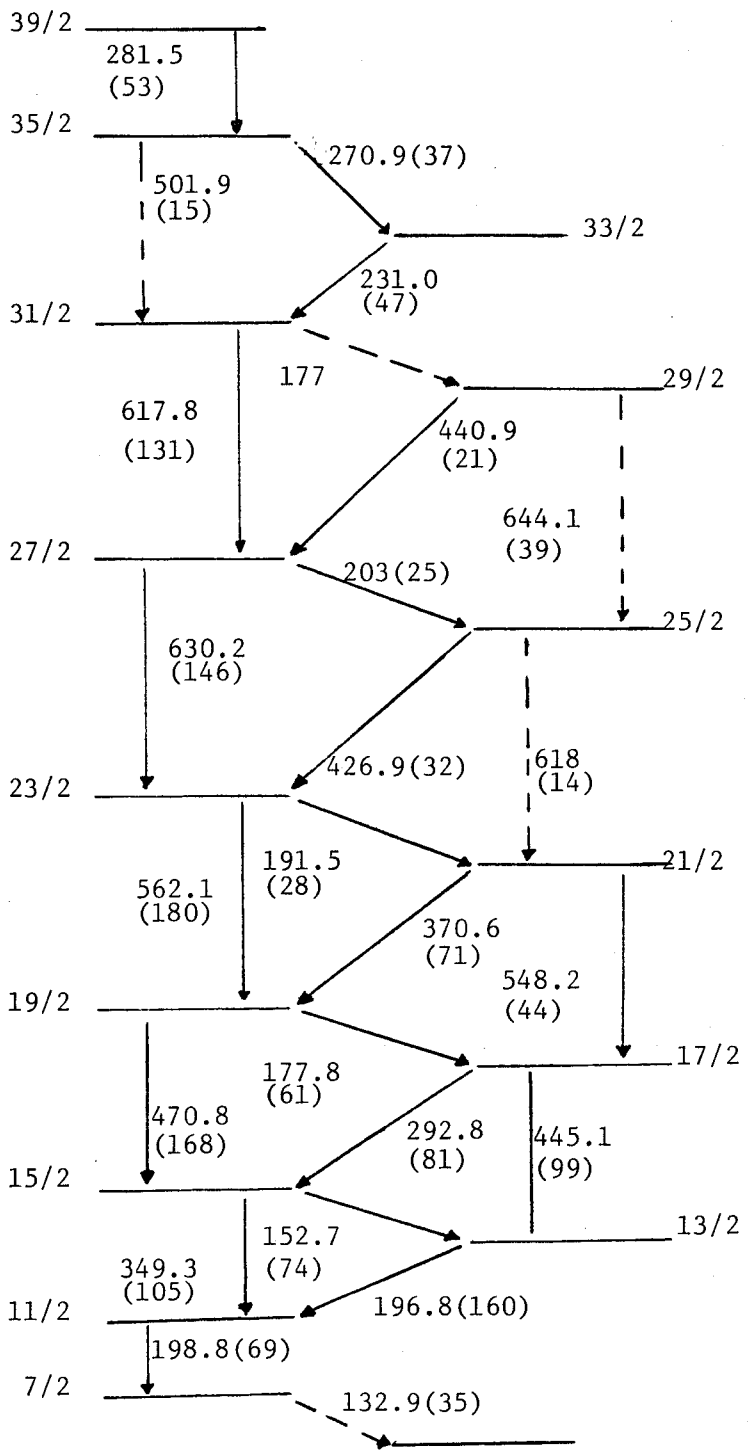

Figure 4.1 The level scheme for Lu-163

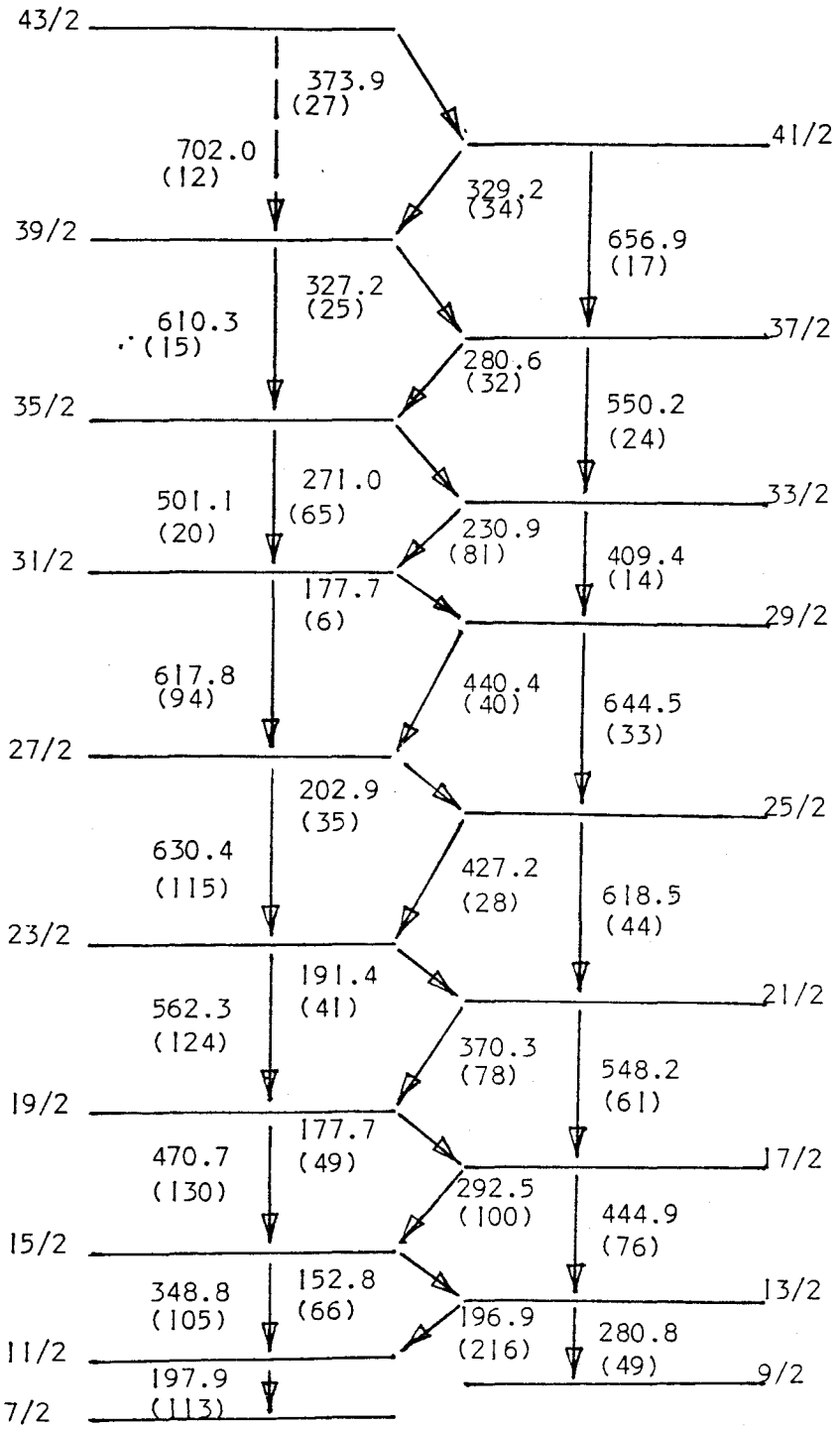

Figure 4.2 The level scheme for Lu-163

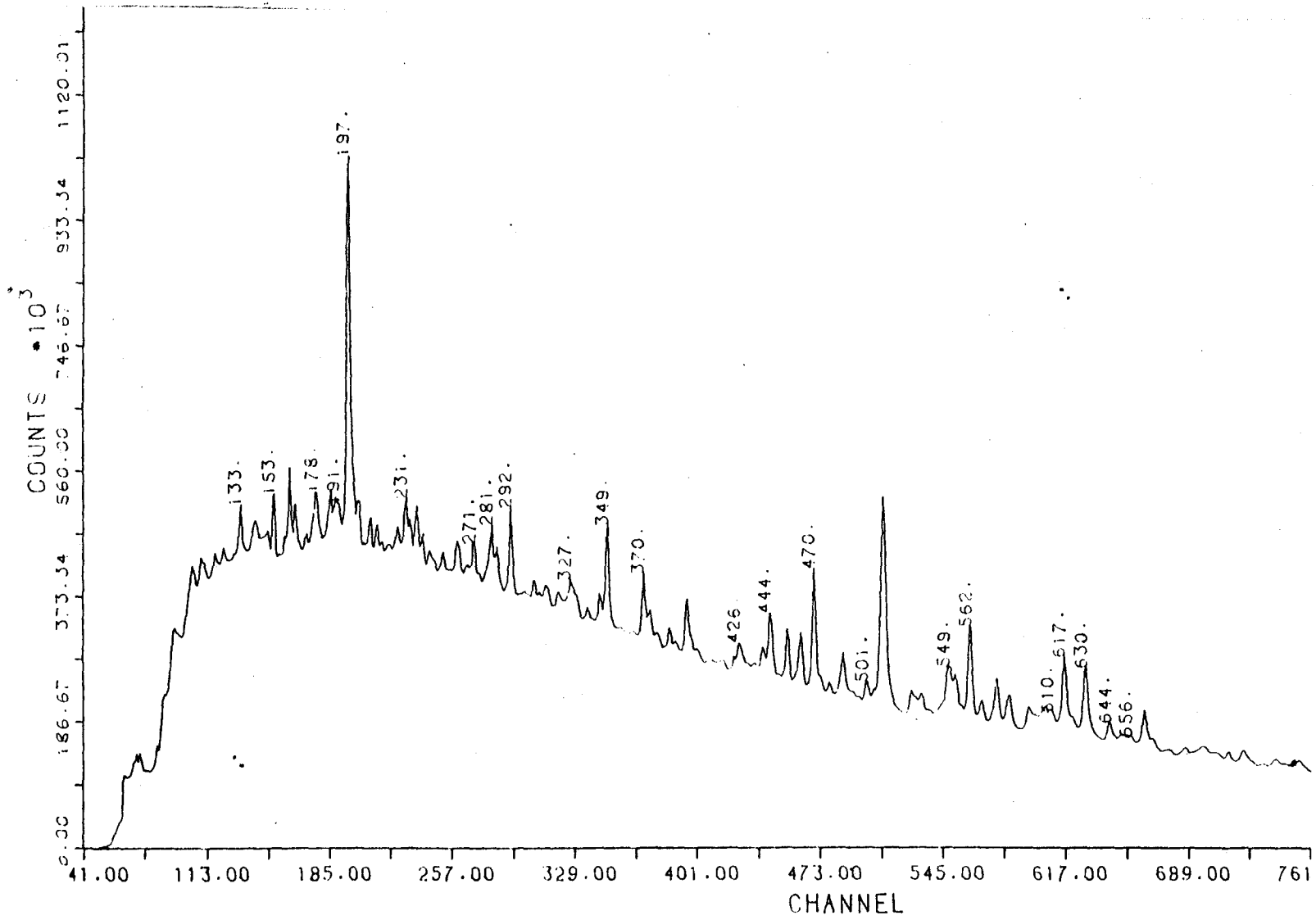

Figure 4.3 The gated singles spectrum.

to give around 0.5 keV per channel, using ^{137}Cs and ^{57}Co sources. An intensity calibration was made using a standard source suitable for the experiment's range, ^{152}Eu, to get the relative intensities for the gamma transitions of ^{163}Lu.

A summary of the results are shown in Table 4.1, where the first column shows the energies of the gamma transition, the second column shows their relative intensities, and the third column shows the assigned initial, $[I]^{\Pi}$, and final, $[I-1]^{\Pi}$ or $[I-2]^{\Pi}$, spins for each level. In analogy with other nuclei in these regions, the yrast cascade has been assumed to be the $h_{11/2}$ band.

4.3 The Gamma-Gamma Coincidence Results

The gamma-gamma coincidence spectrum is a record of all the gamma ray energy transitions coming in coincidence with another gamma ray energy transition, named the gate, and represents a relation of the number of counts per channel and the energy.

Figures 4.4 to 4.13 are a sample of the coincidence spectra associated with the gates studied with the experiment. These background subtracted spectra illustrate the quality of the data and support the level scheme in Figure 4.2. A partial level scheme, with the area of the gate and the gamma energy transitions closely associated with the gate,

TABLE 4.1

ENERGY keV	RELATIVE INTENSITY	ASSIGNMENT
152.817±0.2	66±1	$15/2^- \rightarrow 13/2^-$
177.696±0.2	49±3	$19/2^- \rightarrow 17/2^-$
	6±3	$31/2^- \rightarrow 29/2^-$
191.417±0.2	41±2	$23/2^- \rightarrow 21/2^-$
196.933±0.2	216±12	$13/2^- \rightarrow 11/2^-$
197.944±0.2	113±10	$11/2^- \rightarrow 7/2^-$
202.917±0.2	35±2	$27/2^- \rightarrow 25/2^-$
230.906±0.2	81±1	$33/2^- \rightarrow 31/2^-$
270.970±0.2	65±1	$35/2^- \rightarrow 33/2^-$
280.619±0.2	49±3	$13/2^- \rightarrow 9/2^-$
	32±3	$37/2^- \rightarrow 35/2^-$
292.499±0.2	100±1	$17/2^- \rightarrow 15/2^-$
327.218±0.2	25±2	$39/2^- \rightarrow 37/2^-$
329.222±0.2	34±2	$41/2^- \rightarrow 39/2^-$
348.764±0.2	105±1	$15/2^- \rightarrow 11/2^-$
370.320±0.2	78±3	$21/2^- \rightarrow 19/2^-$
373.870±0.2	27±3	$43/2^- \rightarrow 41/2^-$
409.392±0.2	14±3	$33/2^- \rightarrow 29/2^-$
427.215±0.3	28±2	$25/2^- \rightarrow 23/2^-$
440.399±0.2	40±2	$29/2^- \rightarrow 27/2^-$
444.932±0.2	76±1	$17/2^- \rightarrow 13/2^-$

TABLE 4.1 [CONT'D]

ENERGY keV	RELATIVE INTENSITY	ASSIGNMENT
470.707±0.2	130±1	$19/2^- \rightarrow 15/2^-$
501.087±0.2	20±2	$35/2^- \rightarrow 31/2^-$
548.187±0.2	61±2	$21/2^- \rightarrow 17/2^-$
550.191±0.3	24±2	$37/2^- \rightarrow 33/2^-$
562.304±0.2	124±1	$23/2^- \rightarrow 19/2^-$
610.318±0.3	15±2	$39/2^- \rightarrow 35/2^-$
617.834±0.2	94±1	$31/2^- \rightarrow 27/2^-$
618.500±0.3	44±2	$25/2^- \rightarrow 21/2^-$
630.361±0.2	115±1	$27/2^- \rightarrow 23/2^-$
644.492±0.2	33±2	$29/2^- \rightarrow 25/2^-$
656.917±0.2	17±2	$41/2^- \rightarrow 37/2^-$
702.000±0.4	12±3	$43/2^- \rightarrow 39/2^-$

has been attached to each spectrum, to aid in interpreting the spectrum.

To study a coincidence gated spectrum, a good look was taken at the changes of the relative intensities of the gamma energy peaks, with respect to their relative intensities at the singles spectrum.

A discussion of some of the coincidence spectra will follow. This discussion will only illustrate the techniques used and the quality of the data.

1) The coincidence spectrum for an energy 348.8 keV gate is shown in Figure 4.4. The absence of the peak of energy 348.8 keV indicates that the transition is a single transition. The disappearance of peaks of energies 152.8 keV and 444.9 keV shows that these transitions are not in coincidence with the gate energy. The intensity reduction of peak of energy 196.9 keV, (relative to that in the singles spectrum) indicates that this gamma energy is not in coincidence with the gate energy (The 196.9 peak is a doublet with two gamma rays of energy 196.9 and 197.9 keV. The gamma ray of energy 197.9 is in coincidence with the gate energy). Although the peak with energy 280.6 keV is reduced, it hasn't been eliminated completely. This implies that there are two transitions with energy 280.6 keV, one is in coincidence with the gate energy, and the other is not. The relative

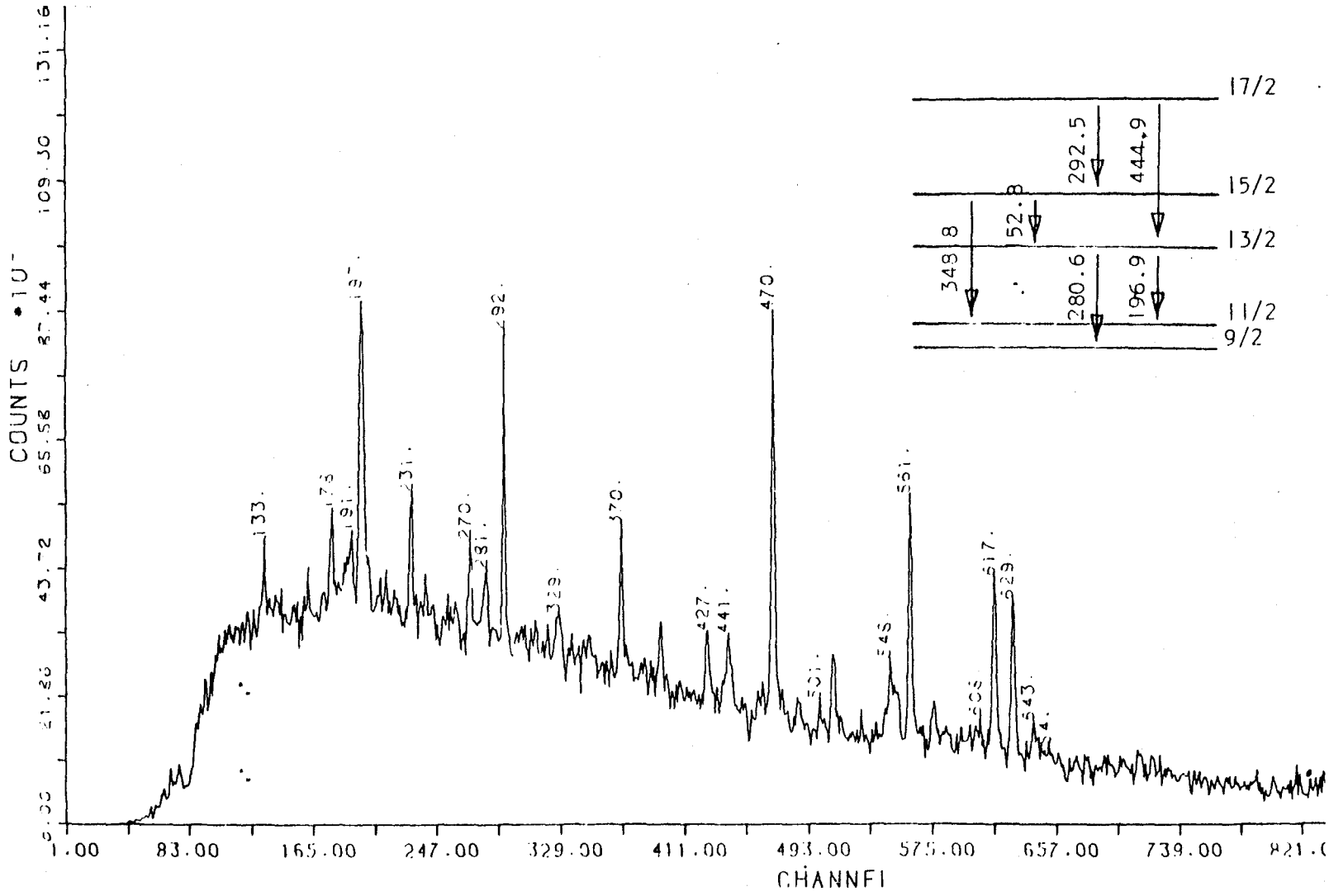

Figure 4.4 The coincidence spectrum for 348.8 KeV

increase of the intensity for peaks of energies 292.5 and 470.7 keV, results from the fact that these t-ransitions are near the gating transitions in the level scheme.

The above arguments support the previously assigned location of the 348.8 keV transition in the level scheme (see Figures 4.1 and 4.2).

2) The coincidence spectrum for the 618.5 keV gate is shown in Figure 4.5. The peak of energy 618.5 keV has not been eliminated from the spectrum (although the intensity is reduced relative to the singles spectrum) which indicates that the 618 line is a doublet. There are two gamma rays of energies 618.5 and 617.9 keV). The disappearance of peaks of energies 562.3, 191.4, 427.2 and 630.4 keV shows that these energies are not in coincidence with the gate energy. The relative increase in intensities of the peaks of energies 644.5, 202.9, 370.3 and 548.2 keV supports the argument that these energies are in close coincidence with the gate energy.

The above indications show that a transition of energy 618.5 keV is consistent with its placing in the scheme.

3) The coincidence spectrum for energy 644.5 keV, is shown in Figure 4.6. The peak of energy 644.5 keV, is obviously a singlet. The disappearance of peaks of energies 202.9 and 440.4 keV indicates

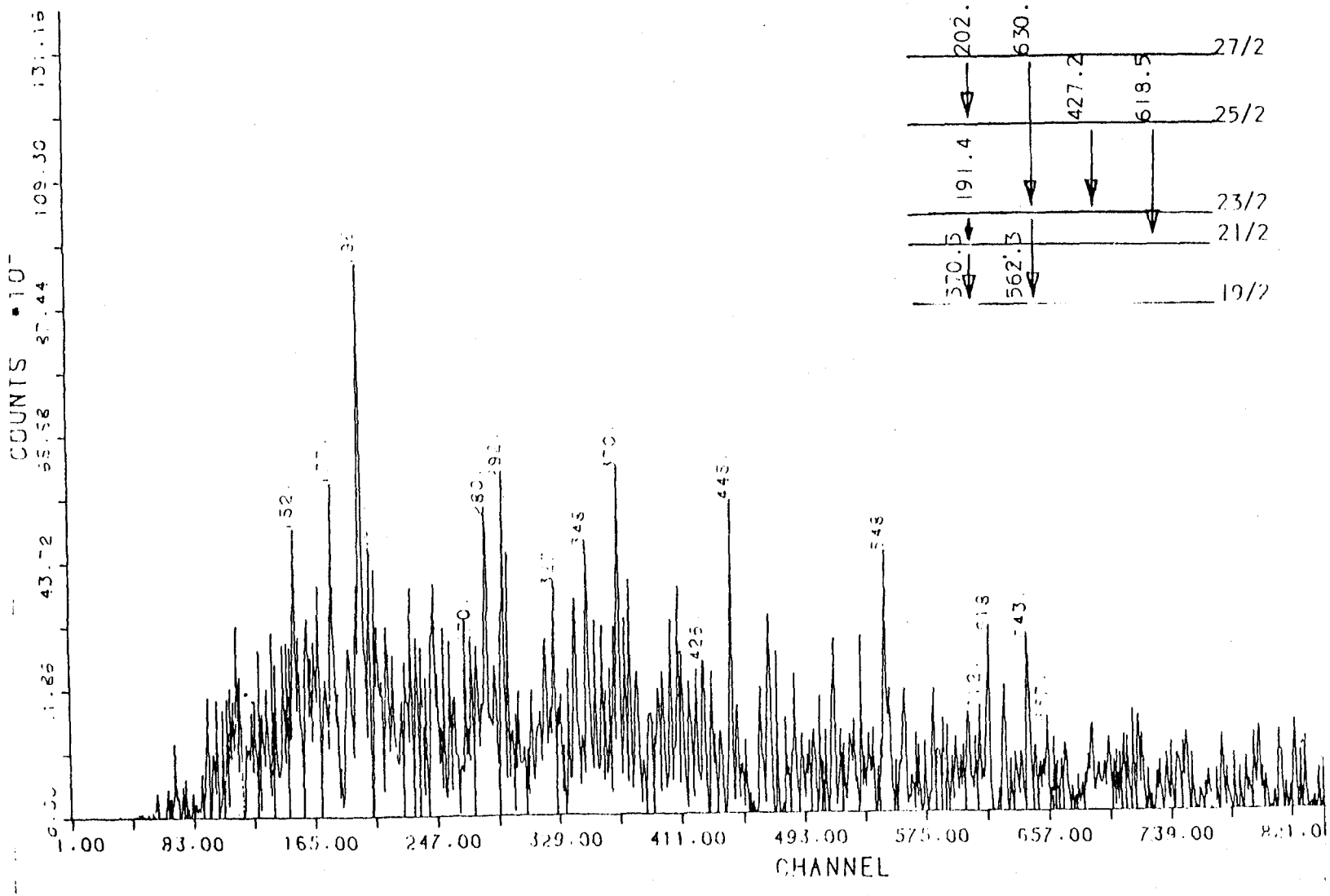

Figure 4.5 The coincidence spectrum for 618.5 KeV

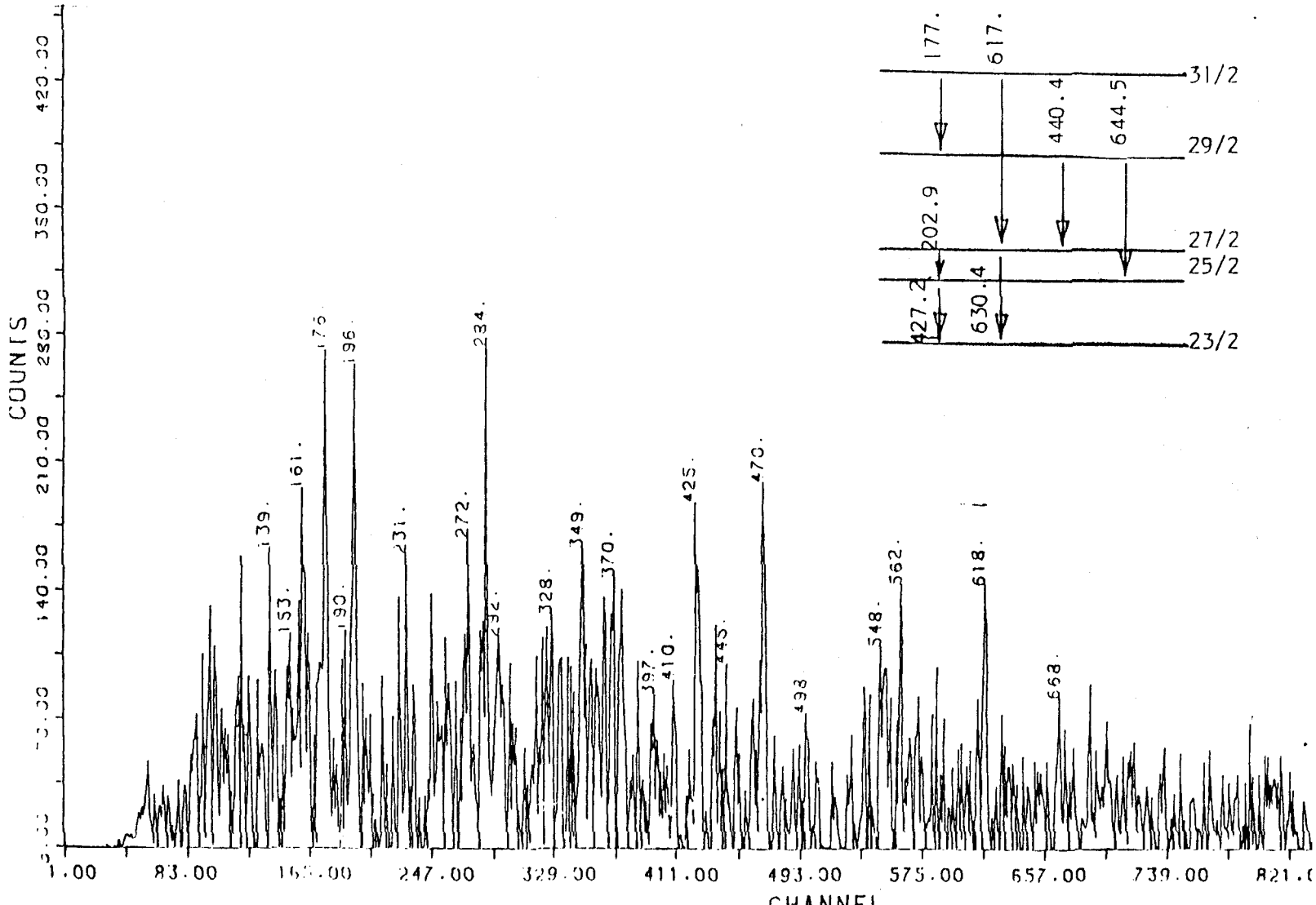

Figure 4.6 The coincidence spectrum for 644.5 KeV

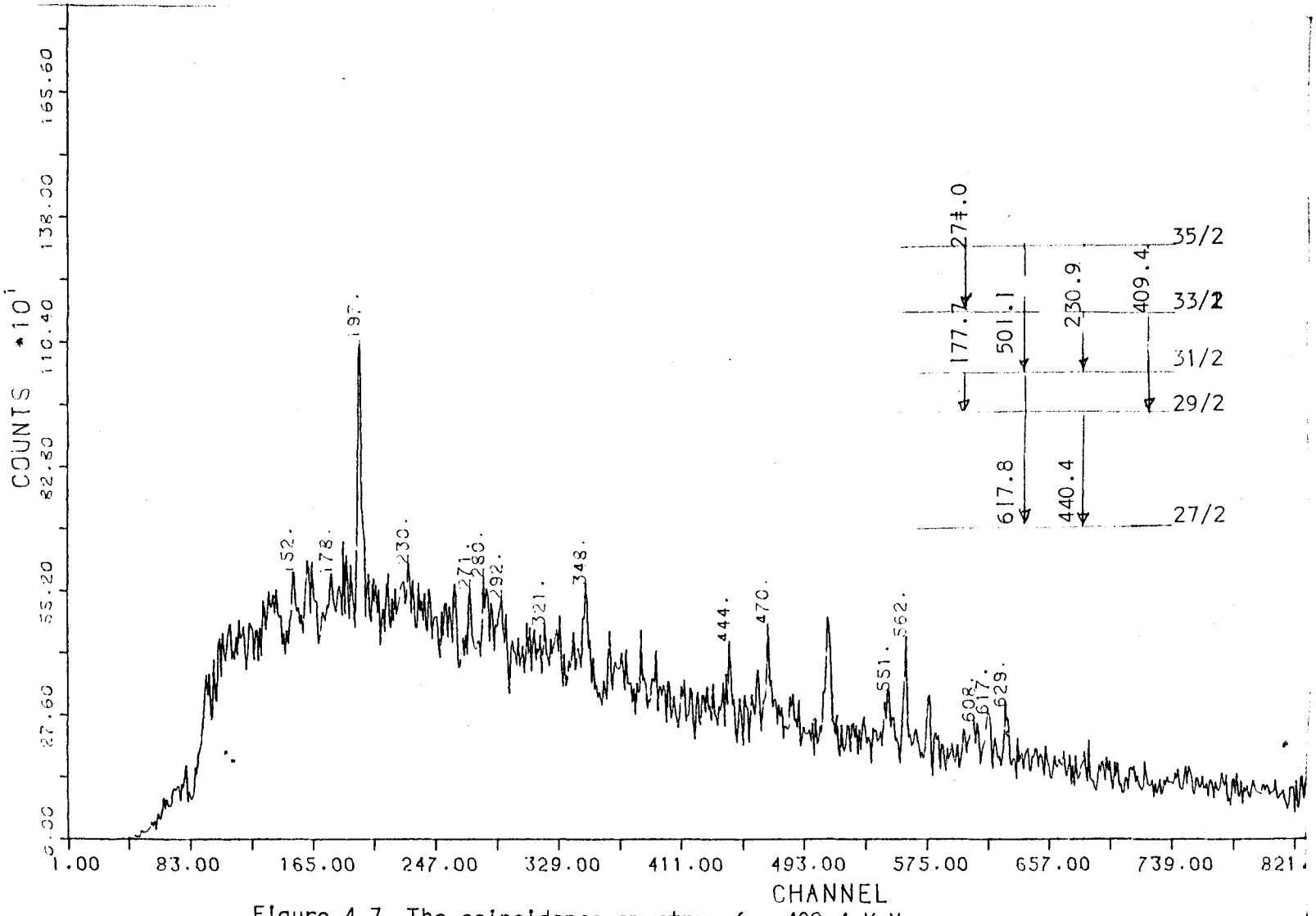

Figure 4.7 The coincidence spectrum for 409.4 KeV

that these energies are not in coincidence with the gate energy. The peak of energy 630.4 keV has been eliminated and is thus in parallel with the gating transition. The intensity increase of peaks of energies 177.7, 409.4 and 427.2 keV shows that these energies are in coincidence with the gate energy and are closely associated in the level scheme. The transition of energy 644.5 keV has been placed between the levels labelled with spins 29/2 and 25/2.

4) The coincidence spectrum for a gamma ray of energy 409.4 keV, is shown in Figure 4.7. The transitions of energies 230.9 and 501.1 keV, are in parallel with the gate and are not in coincidence with the gate transition energy. The intensity increase of the peaks of energies 271.0 and 550.2 keV indicates, that these energies are in coincidence with the gate energy. Thus it is clear that a 409.4 keV transition must be between the levels labelled with spins 33/2 and 29/2. This relatively weak transition was not observed in the previous work.

5) and 6) The coincidence spectra for the 501.1 and 271.0 keV gamma rays (Figures 4.8 and 4.9) are quite straight forward and support the placing of those gamma rays in the level scheme as shown.

7) The coincidence spectrum for a gamma ray of energy 280.6 keV is shown in Figure 4.10. The intensity for the peak of energy 280.6 keV decreased

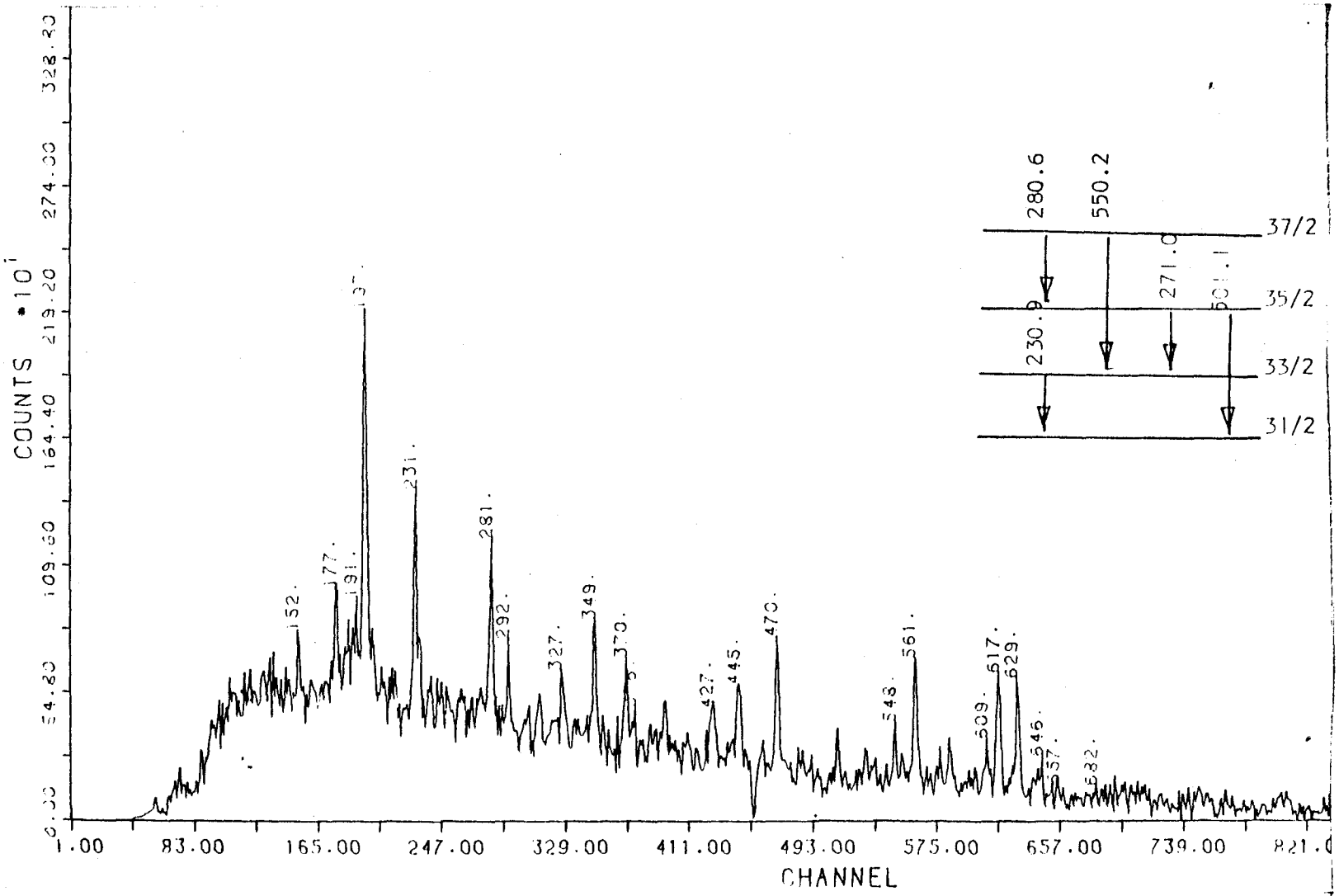

Figure 4.9 The coincidence spectrum for 271.0 KeV

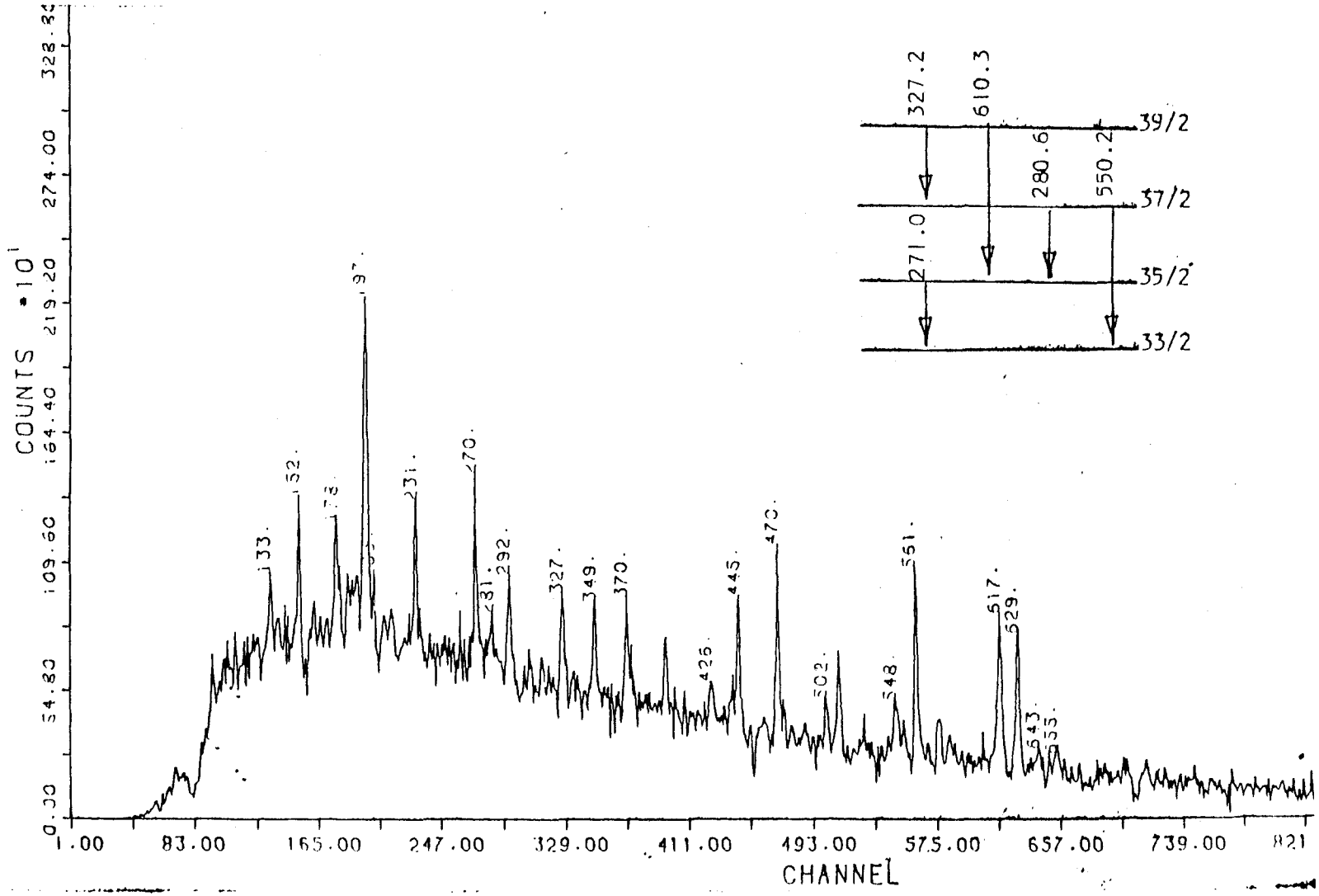

Figure 4.10 The coincidence spectrum for 280.6 KeV

but was not removed completely. Thus there is a coincidence between a pair of 280 keV transitions. One of these transitions disappears, leaving the other (which is in coincidence with the gate energy) to appear. The disappearance of peaks of energies 550.2 and 610.3 keV, indicates that these energies are not in coincidence with the gate energy. However the intensity increase of peaks of energies 271.0, 501.1, 656.9 and 327.2 keV show that these energies lie close to the gating transition in the level scheme.

A transition of energy 280.6 keV has been placed between the levels labelled by spins 37/2 and 35/2. The intensity reduction for peaks of energies 196.9 and 348.8 keV, and the increase of peaks of energies 152.8 and 444.9 keV, lead to the position of the second 280.6 keV transition shown in Figure 4.2. The intensity increase of peaks of energies 152.8 and 444.9 keV indicates, that these energies are in coincidence with the gate energy.

8) The coincidence spectra for some of the highest transitions in the scheme are shown in Figures 4.11 and 4.12. Although these transitions are very weak, the complete evidence is consistent with their placing in the scheme.

9) The coincidence spectrum for a gamma ray of energy 329.2 keV, is shown in Figure 4.13. The

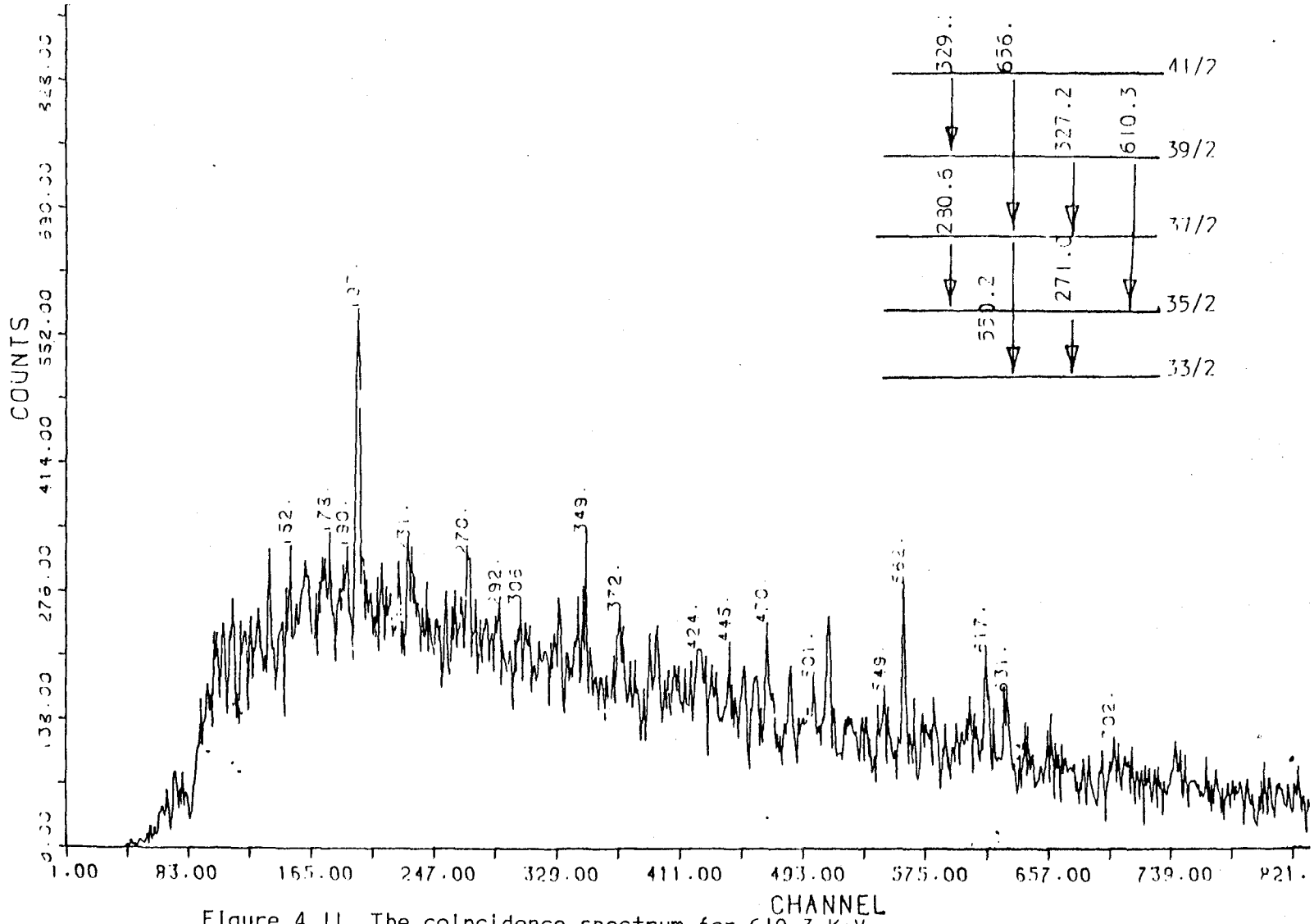

Figure 4.11 The coincidence spectrum for 610.3 KeV

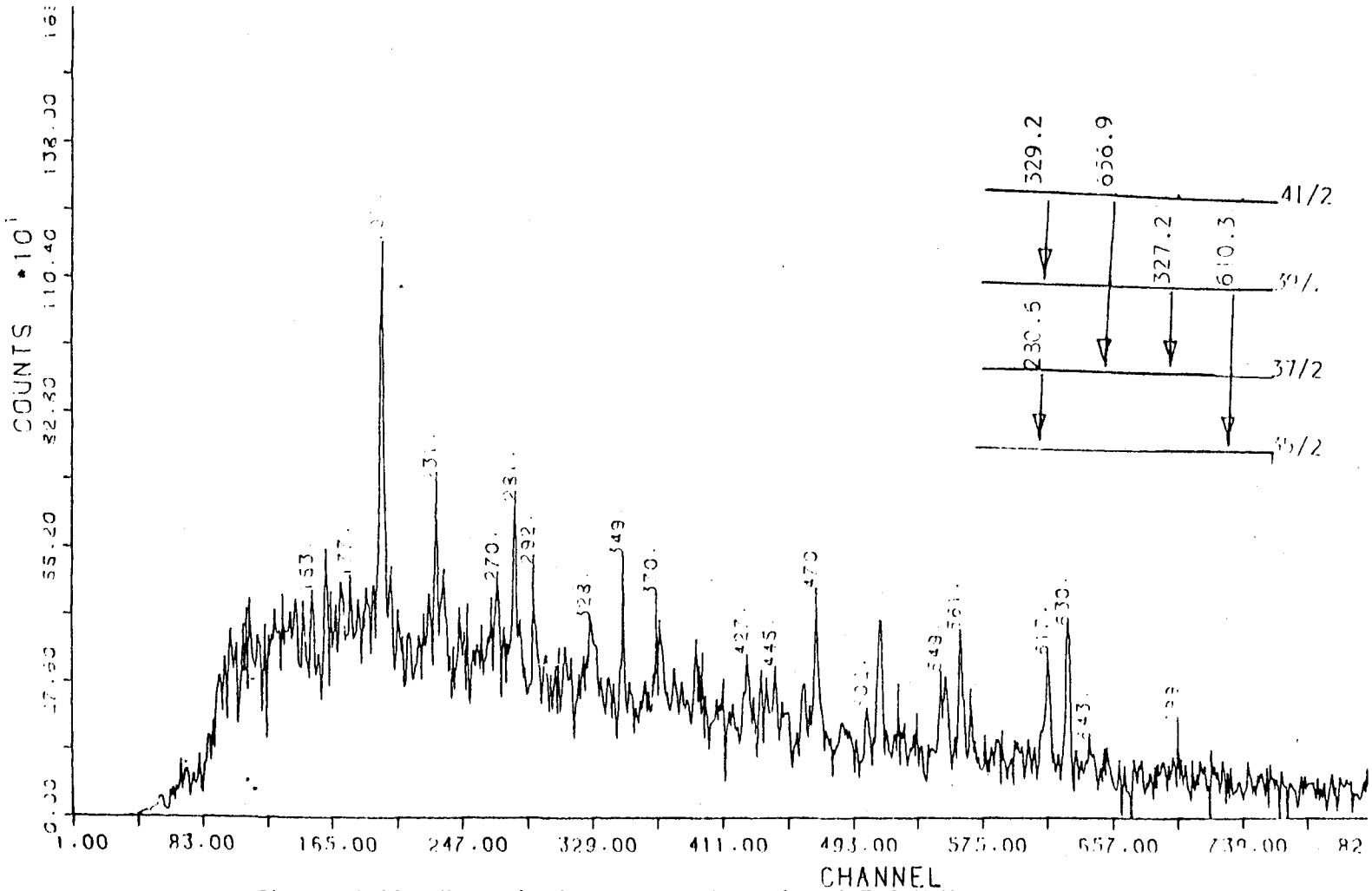

Figure 4.12 The coincidence spectrum for 327.2 KeV

absence of the peak of energy 329.2 keV indicates that it is a single transition. The peaks of energy 656.9 and 702.0 keV, are not in coincidence with the gate but peaks of energies 327.2, 610.3 and 373.9 keV are in coincidence.

From these indications, a transition of energy 329.2 keV must be between levels labelled with spins 41/2 and 39/2.

4.4 The Backbending Behavior Result

The moment of inertia and the rotational frequency for these bands have been calculated from the transition energies in Table 4.2. These parameters are also displayed in that Table and in Figure 4.14. An inspection of this backbending plot, allows two effects to be distinguished:

i) A slow and gradual increase of the moment of inertia at lower angular momenta.

ii) A sudden change of the moment of inertia in the backbending region.

Table 4.3 presents the expectation values for the angular momenta $\langle I_x \rangle$, (third column), for the transitions in the two bands. This expectation value has been calculated using equation 2.15 assuming K = 9/2.

Figure 4.15, is the more modern way to present the backbending behaviour. It shows $\langle I_x \rangle$ vs

TABLE [4.2]

TRANSITION	ENERGY keV	$2\theta/\hbar^2$ [MeV]$^{-1}$	$\hbar^2\omega^2$ [MeV]^2
11/2 - 7/2	197.9	30.2	0.0132
13/2 - 9/2	280.6	35.6	0.0221
15/2 - 11/2	348.8	40.1	0.0323
17/2 - 13/2	444.9	40.4	0.0514
19/2 - 15/2	470.7	46.7	0.0568
21/2 - 17/2	548.2	47.4	0.0765
23/2 - 19/2	562.3	53.4	0.0801
25/2 - 21/2	618.5	55.0	0.0966
27/2 - 23/2	630.4	60.3	0.1002
29/2 - 25/2	644.5	65.2	0.1045
31/2 - 27/2	617.8	74.5	0.0960
33/2 - 29/2	409.4	121.9	0.0422
35/2 - 31/2	501.1	107.7	0.0631
37/2 - 33/2	550.2	105.0	0.0765
39/2 - 35/2	610.3	101.6	0.0934
41/2 - 37/2	656.9	100.5	0.1082
43/2 - 39/2	702.0	99.7	0.1235

TABLE 4.3

TRANSITION	ENERGY keV	$\langle I_x \rangle$	$\hbar\omega$ MeV
11/2 - 7/2	197.9	4.85	0.115
13/2 - 9/2	280.6	6.04	0.149
15/2 - 11/2	348.8	7.18	0.180
17/2 - 13/2	444.9	8.28	0.227
19/2 - 15/2	470.7	9.35	0.238
21/2 - 17/2	548.2	10.42	0.277
23/2 - 19/2	562.3	11.47	0.283
25/2 - 21/2	618.5	12.51	0.311
27/2 - 23/2	630.4	13.55	0.317
29/2 - 25/2	644.5	14.58	0.323
31/2 - 27/2	617.8	15.60	0.310
33/2 - 29/2	409.4	16.63	0.206
35/2 - 31/2	501.1	17.65	0.251
37/2 - 33/2	550.2	18.67	0.277
39/2 - 35/2	610.3	19.69	0.306
41/2 - 37/2	656.9	20.7	0.329
43/2 - 39/2	702.0	21.71	0.351

ω for the $\alpha = -1/2$ and $\alpha = 1/2$ signatures of the $h_{11/2}$ band in ^{163}Lu.

4.5 Aligned Angular Momentum

For understanding the relationships in rapidly rotating nuclei, the rotational frequency, ω plays the crucial role. Figures 4.14 and 4.15 show plots constructed from the experimental data in Tables 4.2 and 4.3. Following the yrast level sequence, the backbending curve is clearly seen. The occurence of this effect reflects the crossing of levels belonging to two bands with different aligned angular momenta. In the data of Figure 4.2, the two bands are identified, both before and after the crossing. The angular momentum for the S-band for a given frequency is considerably greater than that of the ground band.

The difference $\Delta i(\omega) = I(\omega) - I_g(\omega)$ between the excited band and the ground configuration is an important physical property, which plays an important role in the classification and interpretation of the excited bands. The angular momentum $\Delta i(\omega)$ reflects the tendency of the Coriolis force to align the angular momentum with respect to the direction of the total angular momentum.

This gain in alignment Δi has been found to be 7h and 8h for the $\alpha = -1/2$ and $\alpha = 1/2$ signatures respectively. This may be compared with the 9.6 and

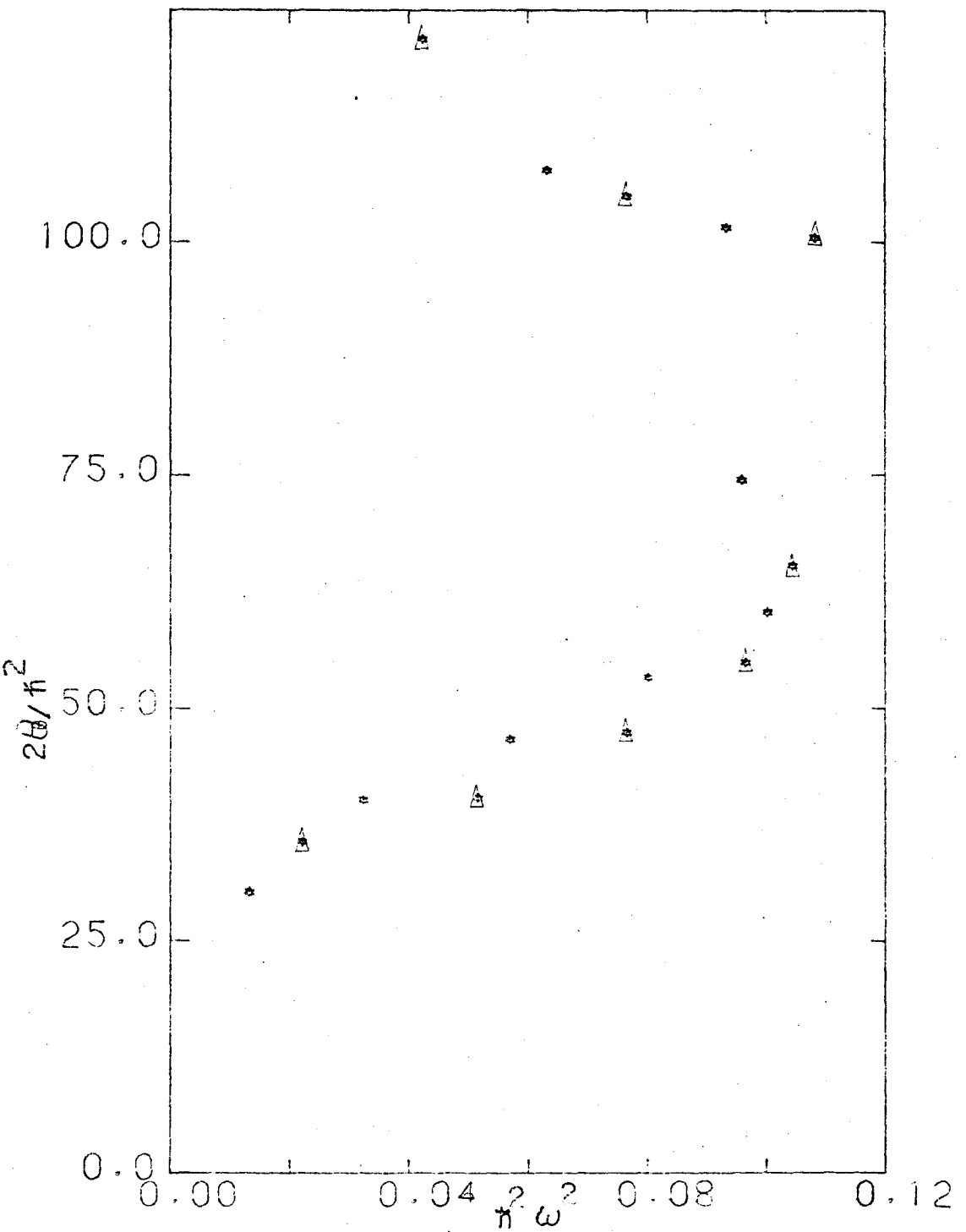

Figure 4.14 The moment of inertia vs the square of the angular frequency.

" △ for $\alpha = \frac{1}{2}$ and * for $\alpha = -\frac{1}{2}$ "

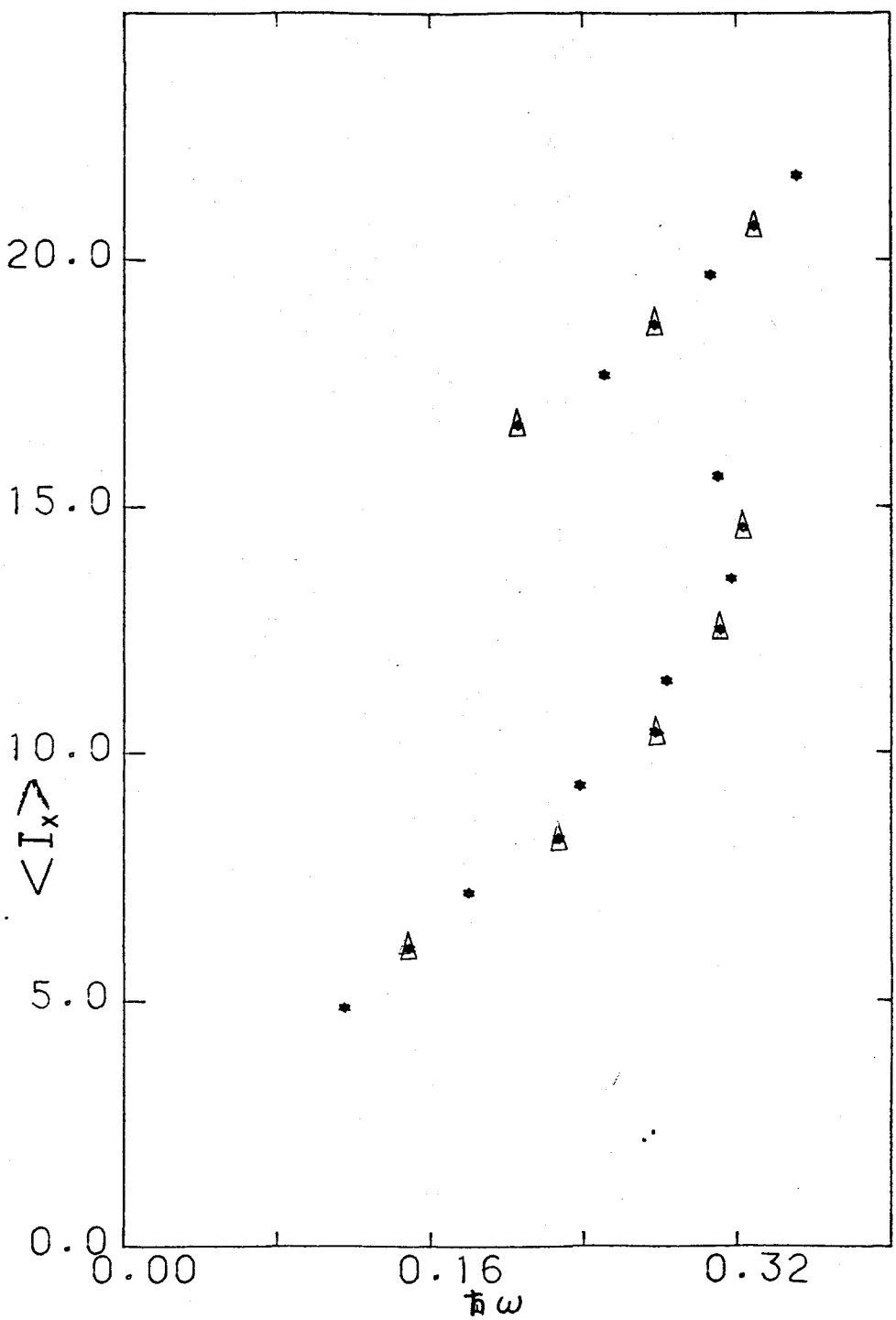

Figure 4.15 The expectation value of the angular momentum vs the angular frequency.

10.2 h observed in ^{159}Tm by Larabee. The addition of a pair of protons and a pair of neutrons has reduced the gain in alignment.

The crossing frequencies have been measured to be $h\omega_c$ = 0.28 and 0.26 MeV which are exactly the same frequencies found in ^{159}Tm.

CHAPTER [5]

CONCLUSION

The results presented in Chapter 4 show the following about the $h_{11/2}$ band in ^{163}Lu.

1. In the present work, more information about the two bands, $\alpha=-1/2$ and $\alpha=1/2$, has been found, up to levels labelled with spin of 43/2 and 41/2 for each band respectively as in Figure 4.2.

2. The transitions of energy 618.5, 644.5, 177.7, and 501.1 keV were shown as doubtful transition in the previous work (Figure 4.1). These transitions have been studied carefully, and have been assigned to their positions. A transition of energy 280.6 keV, Figure 4.1, has been assigned previously to be between levels of spins 39/2 and 35/2. The present work indicates that, there are two transitions with an energy of 280.6 keV, and they have been assigned to be between levels of spins 13/2 and 9/2, and 37/2 and 35/2.

3. A number of transitions involving the highest spin states has been assigned as shown in Figure 4.2.

4. The results presented in Tables 4.1 and 4.2, and Figures 4.13 and 4.14, show the backbending

behavior for ^{163}Lu bands. As described in Chapter 2, this backbending behavior comes as result of the decoupling of a pair of nucleons (the $i_{13/2}$ neutrons) (the $h_{11/2}$ single proton) from the core rotation, and aligning their angular momentum in the direction of the axis of rotation. The increase in the momentum of inertia occurs at frequencies of $\hbar\omega_c$ = 0.28 and 0.26 MeV for the two signatures. The gains in alignment, Δ_i, are 7 and 8h. These values are less than those found by Larabee and Waddington in ^{159}Tm.

5. There was an interference for some energies, which led to some difficulty in determining the relative intensities, and for some time, in interpreting the coincidence spectra, these transitions come from other bands within the ^{163}Lu nucleus. As yet the structure of these bands has not been determined.

A prominant feature of the level scheme is the difference in transition rates before and above the backbend. Above the backbending the transitions from I to I-1, have more intensity than those from I to I-2.

The present work presents some information about two bands and the backbending behavior for the ^{163}Lu nucleus, which could help for futher studies.

REFERENCES

G.D. Alkhazov et al, Z. Phys. A291, 397 (1979).

E.Y. Berlovich et al, Acta Physica Polonica, vol. B11, 455 (1980).

A. Bohr and B.R. Mottelson, Physica Scripta, 10A, 13 (1974).

A. Bohr and B.R. Mottelson, Physics Today, June 1979, 27.

A. Bohr and B.R. Mottelson, J. Phys. Soc. JAPAN 44 (1978) 157-172.

A.J. Larabee and J.C. Waddington, Phys. Rev. 24, 2367 (1981).

R.M. Lieder and H. Ryde, Advances in Nuclear Physics, vol. 10 (1978).

M.A.J. Moriscotti, G. Scharff-Goldhaber and B. Buck, Phys. Rev. 178 (1969).

L. Richer, H. Backe, E. Kankeleit, F. Wiek and R. Willwater, Phys. Letts. 71B, 74 (1977).

L.L. Riedinger, Physica Scripta, 24, (1982).

M.S. Rosenthal et al, Conference.

R.A. Simon, Rev. Mod. Phys. 45, 353 (1973).

F.S. Stephens and R.S. Simon, Nucl. Phys. A183, 257 (1972).

F.S. Stephens, R.M. Diamond and S.G. Nilsson, Phys. Lett. 44B, 429 (1973).

F.S. Stephens, Rev. Mod. Phys. 47 (1975).